AIAA Aviation
16-20 June 2014, Atlanta, GA
20th AIAA/CEAS Aeroacoustics Conference

Specification of Porous Materials for Low-Noise Trailing-Edge Applications

M. Herr, K.-S. Rossignol*, J. Delfs†
German Aerospace Center (DLR), D-38108 Braunschweig, Germany
M. Mößner‡ and N. Lippitz§
Technical University of Braunschweig, D-38108 Braunschweig, Germany

Systematic testing of the microstructural and aeroacoustic properties of porous metals applicable as low-noise trailing-edge (TE) treatments has been initiated within the Collaborative Research Center *SFB 880—Fundamentals of High-Lift for Future Civil Aircraft*. Generic TE noise experiments were performed at $Re = 0.8 \times 10^6$ to 1.2×10^6 in DLR's open-jet AWB facility. Complementary flow measurements in the closed test section MUB wind-tunnel of the TU Braunschweig served to quantify the induced aerodynamic effects. The presented database forms part of an ongoing cumulative effort, combining experimental and numerical methods, to gain a deeper understanding of the prevalent TE noise reduction mechanisms. For the large variety of porous materials tested herein a clear dependence of the achieved broadband noise reduction (reaching 2–6 dB at maximum) on the flow resistivity was identified. Basic design recommendations for material resistivity and pore sizes, the latter to minimize high-frequency self-noise contributions, were deduced for low-noise TE applications. An acoustic nearfield pressure release across the porous region, adversely coupled with a loss in lift performance for porous TE replacements, appears as the major noise-reduction requirement.

Nomenclature

Parameter Definition and Units

b	m	wetted airfoil span
c_l	-	lift coefficient
c_p	-	static pressure coefficient
d_i	m	specific dimensions to characterize porosity; for indices $i = f, p, s$ refer to Table 1
f_m	Hz	1/3-octave band center frequency
h	m	trailing-edge thickness
$L_{p(1/3)}$	dB	1/3-octave band farfield trailing-edge noise level (re 20 μPa)
$L_{p(1/3)norm}$	dB	normalized 1/3-octave band farfield trailing-edge noise level (re 20 μPa)
l_c	m	chord length
l_p	m	length of pores/slits
M_∞	-	free-stream Mach number
$\langle p'^2 \rangle$	Pa	mean-square sound pressure
R	Ns/m^4	specific flow resistivity, referenced to the functional layer thickness, $R = R^0/t$
R^0	Ns/m^3	specific (ac or dc) flow resistivity, $R^0 = \Delta p_0/u_0$

*Research Scientists, DLR Institute of Aerodynamics and Flow Technology, Technical Acoustics, Lilienthalplatz 7, michaela.herr@dlr.de, karl-stephane.rossignol@dlr.de, AIAA Members.
†Head of Technical Acoustics Department, DLR Institute of Aerodynamics and Flow Technology, Lilienthalplatz 7, jan.delfs@dlr.de, AIAA Member.
‡Research Scientist, Institute of Fluid Mechanics, Technische Universität Braunschweig, Hermann-Blenk-Str. 37, m.moessner@tu-braunschweig.de.
§Research Scientist, Institute for Materials, Technische Universität Braunschweig, Langer Kamp 8, n.lippitz@tu-bs.de.

R^0_{TE}	Ns/m^3	hypothetic specific flow resistivity for TE applications, cf. p. 8
r	m	distance between source and observer
Re	-	chord-based Reynolds number
Sr	-	Strouhal number
t	m	thickness of the functional layer
u_0	m/s	characteristic (mean or rms) flow velocity
u_∞	m/s	free-stream mean velocity
w_p	m	width of pores/slits
x_1	m	chordwise coordinate
α	°	aerodynamic angle-of-attack
α_{WT}	°	geometric (wind-tunnel) angle-of-attack
Δp_0	N/m^2	(static or rms) pressure drop across a test sample
δ_0	m	characteristic scaling length
δ_{PS}	m	turbulent boundary-layer thickness at the airfoil pressure side (PS)
δ_{SS}	m	turbulent boundary-layer thickness at the airfoil suction side (SS)
ϕ	%	porosity, percentage of open-pore volume in a representative sample volume

I. Introduction

REDUCTION of today's aircraft noise emissions is a desirable socio-political goal. This objective will gain further importance if the airplane exhibits short take-off and landing capabilities to make use of available capacities of small city airports close to densely populated residential areas. In this context the Collaborative Research Center *SFB 880—Fundamentals of High-Lift for Future Civil Aircraft*[1] funded by the *Deutsche Forschungsgemeinschaft* (DFG) focuses on the associated technologies while addressing the following tasks:

1. noise reduction technologies (configuration design and application of porous material),
2. active high-lift systems for short take-off and landing (Coanda flaps and droop nose devices),
3. resulting flight dynamics for the proposed technologies.

The current report concentrates on the first item, addressing the aeroacoustics of porous treatments applied at the trailing-edge (TE) of lifting surfaces. Application of porous material (foams or fibrous material) at high-lift system components has the potential to reduce classical edge-scattering noise,[2] as induced by the turbulent boundary-layers or shear layers originating from powered-lift systems. Up to now, the underlying noise reduction mechanisms are not fully understood and current data bases lack a complete description of actual material properties. Major research objectives were therefore

- to verify the noise reduction benefit of downselected material samples with strong relation to material specifics,
- to provide validation data describing the effect of well-documented porosity on TE noise to support the further-development of current CFD and CAA prediction capability.

In the long term this data base shall be used to validate enhanced numerical models being under development in the SFB 880 that include the effects induced by material porosity in the predictions.

I.A. State of Knowledge—Edge-Noise Reduction by Means of Porous Treatments

Published experimental and numerical efforts to apply flow-permeable material to components of high-lift systems comprised mainly generic studies at model-scale on e. g. slat TE treatments,[3,4,5,6,7a] flap TE treatments,[3,4] and flap side-edge treatments.[3,4,8,9,10,11] Other application areas include edge modifications to

[a] Refs.[5,6] are numerical studies at model-scale slats with blunt TE tonal noise artefacts representing the major source mechanism. The documented noise reduction potential is accordingly narrowband in nature and not related to broadband edge scattering noise. Ref.[7] addresses the effect of porous liners located in the slat cove and leading edge region of the main wing. The underlying model approach extracts only acoustic absorption processes in the nearfield while potential effects of the porosity on the turbulence are not considered.

reduce TE noise of powered-lift configurations,[12,13] turbomachinery blade noise,[14,15] rotor-stator interaction or tip clearance noise,[16] etc.

Early studies on porous edge devices in the 1970s[12,13] addressed the TE noise reduction related to powered-lift applications, and thus, were limited to specific test setups with a small-sized exhaust jet flow impinging on one side of a flat plate[12] or deployed USB flap.[13] For such single-sided jet flow applications porous TEs provided a significant broadband noise reduction, its maximum reaching 10 dB or more. Measured attenuations were equal over a wide range of radiation angles.[12,13b]

A noteworthy early (1968) study on flow-permeable TE treatments at 2D airfoil sections placed in an open-jet flow field, comparable to a typical acoustic wind-tunnel measurement situation (but much smaller in scale), is the one of Potter,[15] building upon the preparative work of Lowson.[14] Addressing applications for compressor blades, more than 20 different TE modifications were investigated in a systematic approach. Therein, most of the currently known and today revisited concept variations were already anticipated (like e. g. a slotted TE design, or porous sheet metal enclosing a hollow TE region). Parameter selection in these early tests was rather arbitrary, but nevertheless, revealed an overall noise reduction of about 3 dB for the most effective configuration. From today's perspective the used test setup—using single farfield microphones for the acoustic measurements—was not suitable to extract TE noise contributions from extraneous facility-related noise to derive reliable parametric test data. It is suspected that the free-jet shear-layers were producing both leading and TE noise contributions of much higher intensity, in particular in the low-frequency range, than the TE noise in this study.

Concluding from a literature review of currently available parametric studies where perforated sheet metal or foam materials were applied for edge noise reduction,[11,12,17,18,19,20] general noise prediction capability can not be provided to date. In more recent experiments on porous 2D SD7003 airfoil sections[17,18,20] no simple parametric relationships could be identified, but a rather unsystematic acoustical behavior.[c]

From another 2D airfoil experiment at a 2D NACA0012-derivative airfoil equipped with porous sheet or cloth material in the TE region[19] no definite design guidelines could be derived due to limitations of the test parameter range in this study.[d] In these recent 2D airfoil experiments maximum overall TE noise reductions of order 3–4 dB were observed for the most beneficial parameter combinations.[18,19] Similar to TE serrations porous materials also involve the risk of additional excess noise generation due to an improper installation and/or due to the perforates' surface roughness and layout (drilled holes provide additional small-scale edges). Moreover, the pressure distribution of the airfoil and accordingly, the turbulent boundary-layer (TBL) properties can be influenced due to cross-flow through the porous material.[19] Geyer et al.[18] measured an artificial thickening of the TBL at both the pressure and suction sides which was likely caused by an increased surface roughness of the porous material, when compared to the (hydraulically smooth) solid reference airfoil. The summation of effects limits the overall data comparability and effective interpretation of results. Correspondingly, no clear universal functional relationship between material properties, flow characteristics and noise reduction benefit can be extracted from the cited studies. At least the main common trends among published test data, hypothesized low-noise design fundamentals and by now unsolved questions are summarized in the remainder of this section. This detailed discussion has its main focus on TE treatments and is supplemented by major theoretical/numerical results. Other edge applications are not specifically addressed herein.

First of all, the governing parameters have to be identified for an optimal material selection. In most of the cited studies the specific (dc and/or ac)[e] airflow resistivity R^0 is taken to quantify the material behavior.

[b] Quantified (> 10 dB) noise reductions refer to single microphone measurements in the acoustic farfield. TE noise directivity data for porous TE treatments could be provided due to sufficient signal-to-noise ratios (S/N) for these specific test conditions with zero mean flow around the jet/flap configuration.

[c] Based on a dimensional analysis approach Sarradj & Geyer[20] / Geyer et al.[17,18] investigated the noise scaling behavior of entirely porous airfoils at small scale, however, with the inherent problem that the influences of concurrent wind-tunnel free-jet shear-layer / airfoil interaction noise, airfoil surface roughness noise, and TE noise sources can not be clearly separated in the achieved noise reduction results.

[d] These tests, conducted in the framework of the EC-cofinanced OPENAIR project, were rather a proof of concept for selected duo-layer mesh materials which had been before positively evaluated by industrial partners with regard to airworthiness requirements. To facilitate retraction of the wing components it was intended to essentially retain the original TE contour when applying flow-permeable material in the TE region. Therefore, the combination of a supporting structure (e. g. a coarse metal mesh/perforated sheet metal or frame structure) to provide stability with a thin, flow-permeable cover material (e. g. a cloth material, micro-perforates or a fine metal weaving) to avoid perforates' self-noise was selected as an applicable innovative solution for a TE noise reduction treatment.

[e] For small frequencies f the dc quantity is expected to apply also to ac fluctuating flow velocities, i. e. for small velocities u_0 also to the acoustic particle velocities in a sound field. Equivalent ac acoustic flow resistivity R^0 of the material is generally

$R^0 = \Delta p_0/u_0$ is typically determined by measurements of the (static or rms) pressure drop Δp_0 across a test sample installed in a tube at selected constant (mean or rms) flow velocities u_0. Suitable measurement methods for R^0 are recommended in DIN EN 29053 (ISO 9053). R^0 is consistently determined by detailed geometric material specifications; for perforated sheet metal materials these are e. g. the size, shape and distribution pattern of the pores, and the resulting porosity. The most frequently used parameters for the characterization of open-cell foam material are the porosity, the average amount and size of the pores in a material cross section, and the tortuosity (a measure for the curvature of the transport paths in a porous material sample, defined as mean effective path length/ sample thickness or as its squared value). In this context it is important to note that the resulting dc R^0 shows a material-dependent non-linear velocity dependence, showing approximately constant R^0 values for small u_0 (which for $u_0 \to 0$ m/s translates to ac R^0 for $f \to 0$ Hz), but increasing dc R^0 for larger u_0. For measurement examples the reader might refer to Refs.[19,11] An empirical design optimization process will therefore have to account for the velocity- and frequency-dependence of the ac flow resistivity in the following way: The material is required to be flow-permeable for the smaller, acoustically relevant wall-normal fluctuating velocities in the source area, but impermeable for typical mean flow velocities.[11] The latter would prevent unwanted mean leakage flow through the material and hence, help to preserve the airfoil's lift performance. Experimental data[19,20] supports the conjecture that for sufficient low values of dc R^0 the aerodynamical performance generally decreases with decreasing dc R^0. In summary, an optimal installation is expected to benefit from the non-linear material flow resistivity behavior. Experimental results[19] indicate that there exist at least acoustically effective, however, not yet acoustically optimized solutions to apply porosity at the TEs of lifting surfaces with no measurable aerodynamic penalties. It will have to be evaluated whether the maximum achievable noise reduction of correspondingly selected solutions is large enough to justify technical application.

Moreover, an ideal porous material application in the TE region would require a gradual change of porosity from zero to one. This, of course, cannot be perfectly realized by insertion of a regularly structured material that introduces another surface impedance discontinuity between the solid airfoil and its insertion position to the already existing one between the TE and the ambient air (like e. g. for the realization described in Ref.[19]). However, it is expected that an optimum exists for this kind of installation. Theoretical and supplementing numerical work on the effect of distributed porosity, applied in the TE region of a semi-infinite rigid plate, was provided by Howe[22f]. Assumptions underlying his approach were no viscosity, no vorticity generation due to the through-flow, no unsteady Kutta condition, i. e. no TE vortex-shedding, and—according to Howe the most critical limitation—unaffected turbulence properties within the TBL. Major results were a TBL-TE noise reduction of order 7 dB (due to the pure influence of the adaptation of the surface impedance) and a favorable noise performance for a more gradual adjustment of the surface impedance by continuously increasing the pore density in the downstream direction. The latter leads to a diminished and broadened acoustic pressure signature across the TE.

Of specific interest with regard to technical applications is the resulting velocity scaling behavior of TBL-TE noise for the presence of porous materials at the TE. In a very recent theoretical/numerical study Jaworski & Peake[25] investigated the effect of poroelasticity on TBL-TE noise generated at a semi-infinite flat plate TE. Their work focused on a systematic comparison of the respective limiting boundary conditions, i. e. rigid impermeable, rigid porous, elastic impermeable, and poroelastic conditions. The resulting velocity scaling laws were therein thoroughly discussed. One major outcome was that the derived velocity scaling was highly frequency dependent; for sufficiently low non-dimensional frequencies edge porosity tends to reduce the well-known $\langle p'^2 \rangle \propto {u_0}^5$ law of a solid plate to a weaker $\langle p'^2 \rangle \propto {u_0}^6$ dependence, whereas elasticity leads to an even weaker $\langle p'^2 \rangle \propto {u_0}^7$ law that rapidly changes towards lower velocity exponents than 5 at higher frequencies. The combined condition of poroelasticity shows an intermediate behavior, i. e. a weak $\langle p'^2 \rangle \propto {u_0}^7$ dependence at low frequencies, but a decreasing velocity exponent with increasing frequency. In this respect available measurement data are ambiguous; in Ref.[19] a clear $\langle p'^2 \rangle \propto {u_0}^5$ dependence—excluding high-frequency excess noise contributions from the scaled broadband TBL-TE noise contributions—was documented for all tested

measured in a standing-wave tube. Note that in the acoustic case the pressure drop and through-flow velocity refer to the complex amplitudes of sound pressure and acoustic particle velocity, i. e. to a complex impedance where the ac R^0 is its real part.[21]

[f]Fully porous, non-compact screens have been already considered earlier by Leppington[23] showing that the corresponding scattering properties are equivalent to those of a homogeneous compliant non-compact plate, i. e. expected TBL-TE scattering results correspond to the ones reported in Ref.[24] (assumed $\langle p'^2 \rangle \propto u_0^6$ scaling of TBL-TE farfield noise). However, for practical applications with the requirement to maintain aerodynamic performance, Howe suggests a chordwise porous extent of order of the hydrodynamic length scale of the incident turbulent flow, i. e. a compact perforated TE region.

materials. In the contrary in Ref.[17,18] velocity exponents between 5 and 7 are reported, however with strong self-noise contributions adding up to the actual TBL-TE noise source.

Current and future work will have to address the compatibility of acoustic efficiency with aerodynamical and structural integrability. Requirements on the used materials are a hydraulically smooth surface (to prevent negative effects on the TBLs and to shift excess noise contributions towards low-weighted high frequencies at full-scale), airworthiness, and a negligible impact on the aerodynamic performance.

II. Experimental Setup

II.A. Downselection of Porous Materials

Various different porous metals were selected for systematic parametric testing; according to Table 1 these were microperforated plates (MPP)[g] with a regular arrangement of long or circular holes, as well as sheets from sintered fiber felt (SFF)[h], blocks from sintered spherical bronze powder (SBP)[h] and porous aluminum (PA)[i] with more stochastic pore distributions. Additional slit TE variants (last two lines in the table), as further specified in Section II.B, were taken as idealized low-noise reference configurations to compare the effects achievable by streamwise aligned porosities (with assumed minimum production of self noise due to flow across prodruding structural elements) relative to more isotropic distributions of pores. Geometric parameters for the slit TE variants were arbitrarily selected based on successful previous TBL-TE noise tests on a NACA0012-derivative airfoil.[26,27]

Measurements of the specific flow resistivity R^0 were conducted by the Physikalisch Technische Bundesanstalt (PTB) in Braunschweig using the alternating airflow method (Method B DIN EN 29053, ISO 9053). Accordingly, the herein documented values correspond to ac R^0 for frequencies of 2 Hz and rms velocities $u_0 = 0.5 \times 10^{-3}$ m/s.

As the materials differ in porosity, pore size and pore morphology, a set of additional parameters was selected to characterize their microstructures. Values of the porosity ϕ, thickness t, pore length l_p, pore width w_p, fiber diameter d_f, and sphere diameter d_s were determined with high accuracy from 3D computer tomography (CT) and/or 2D light microscopy images, hence combining the advantages of both imaging methods. CT imaging provides a good overall impression of the material with a precise determination of the porosity ϕ (based on a defect analysis with reliable distinction between open and closed pores), whereas 2D microscopy features a much higher resolution. Example CT images for the different porous material groups are provided in Figure 1.

It was found that the MPP holes expand from the top (surface of treated TE region) to the bottom (interior) side of the plates. That is why Table 1 contains pore dimensions for each side. The SFF sheets consist of a functional surface top layer and a support grid with significantly bigger pores (bottom/ interior side). As the layer with the smallest pores determines the flow resistivity, only the functional layer without the support grid is regarded and the flow resistivity $R = R^0/t$ is given in relation to the thickness t of the functional layer. For the MPP variants t is equal to the plate thickness, whereas for the SBP, PA and slit TE variants t corresponds to the sample thickness (PTB measurements of R) or to the local profile thickness in the TE region (wind-tunnel experiments, as specified below).

II.B. Aeroacoustic Measurements

Acoustic tests were performed in DLR's Acoustic Wind-Tunnel Braunschweig (AWB) which is an open-jet low-noise facility with closed return circuit providing a maximum flow velocity of 65 m/s.[28] The nozzle has a rectangular cross section with a size of 0.8 m by 1.2 m at its exit. The test airfoil was fixed between two acoustically lined side-walls which allow for angle-of-attack variations. This arrangement results in a wetted span between the side-plates of 0.8 m. Originally, the airfoil model provides an original wingspan of 1.3 m allowing for larger aspect ratios in alternative wind-tunnel setups like the one used for the aerodynamic measurements in the MUB (*Modell-Unterschallkanal Braunschweig*) facility of the TE Braunschweig (see below).

The model's cross section is defined by the DLR F16 airfoil geometry with a chord length of 0.3 m (cf. Figure 2). Static pressure measurement instrumentation consists of 50 static pressure taps along a plane

[g] ANDRITZ Fiedler GmbH, Weidener Strasse 9, D-93057 Regensburg, Germany
[h] GKN Sinter Metal Filters GmbH, Dahlienstrasse 43, D-42477 Radevormwald, Germany
[i] Exxentis AG, Schartenfelsstrasse 6, D-5430 Wettingen, Switzerland

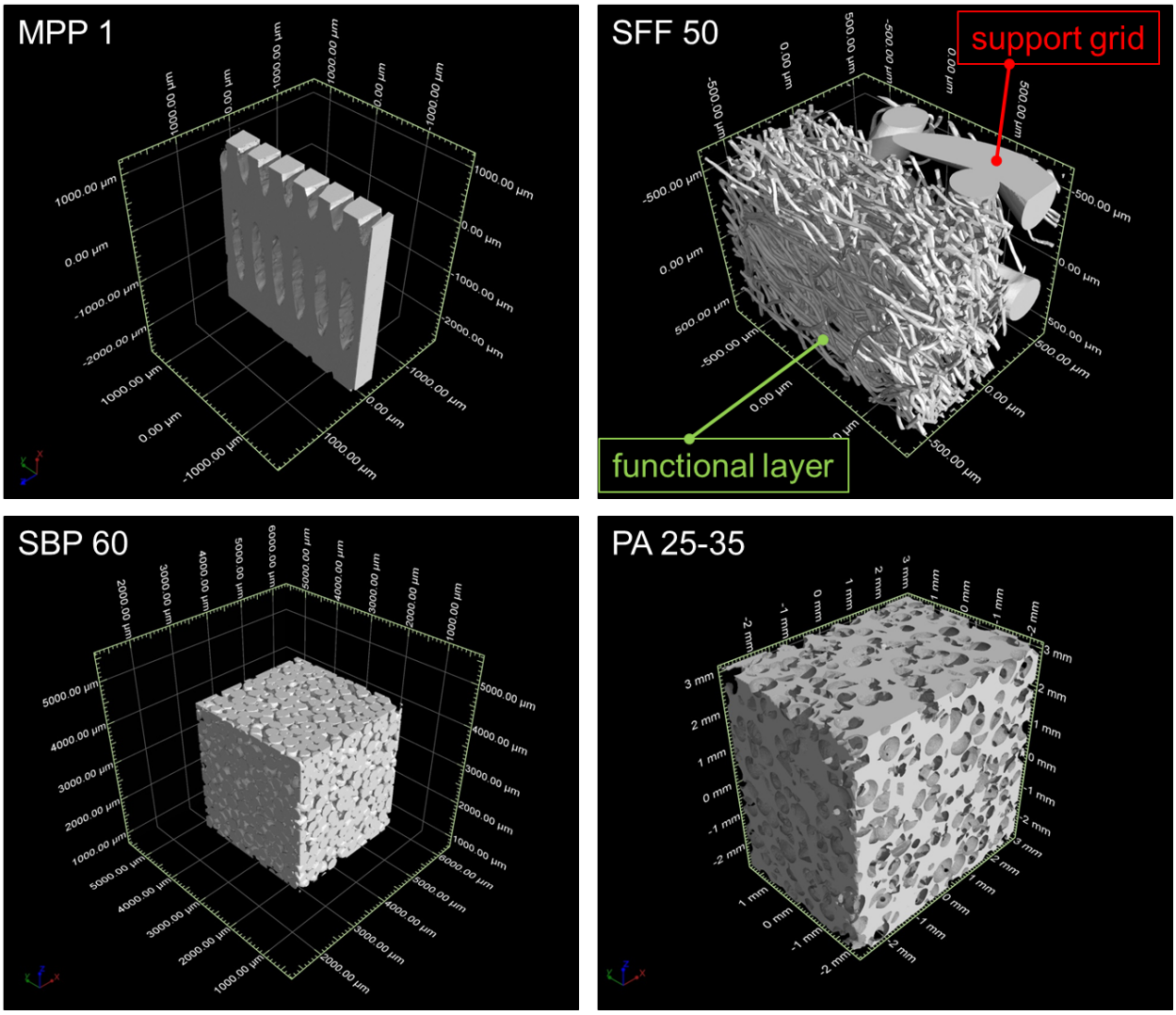

Figure 1. CT images of selected TE material samples.

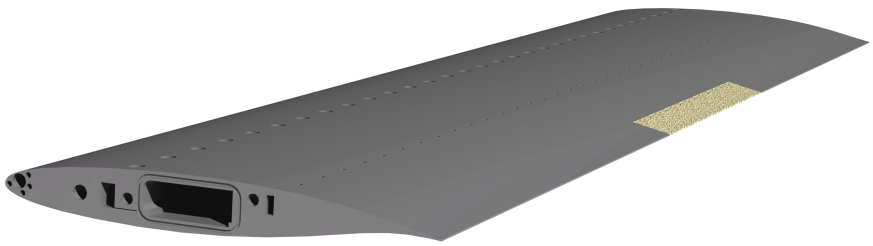

Figure 2. CAD rendering of the airfoil model with solid porous insert installed at the TE.

Table 1. Selected configurations for AWB Tests: microperforated plates (MPP), sintered fiber felts (SFF), sintered bronze powder (SBP), porous aluminum (PA), slotted TEs; porosity ϕ, thickness of the functional layer t, pore length l_p, pore width w_p, fiber diameter d_f, bronze sphere diameter d_s, effective pore size d_p according to single pass test results (ASTM E 1294), specific flow resistivity, referenced to the functional layer thickness ($R = R^0/t$). Values in brackets are estimates or nominal manufacturer's information.

configuration	ϕ, %	t, µm	l_p, µm	w_p, µm	d_i, µm	d_p, µm	R, Ns/m^4
reference	(0)	(TE)	(0)	(0)	-	(0)	(∞)
MPP 1 - top	14	490	1100	100	-	-	88463
MPP 1 - bottom			1400	260	-	-	
MPP 3 - top	18	640	100	100	-	-	234844
MPP 3 - bottom			160	160	-	-	
MPP 4 - top	14	550	60	60	-	-	767291
MPP 4 - bottom			120	120	-	-	
SFF 50	86	590	-	-	25 ($i = f$)	(50) 51	115703
SFF 120	89	270	-	-	26 ($i = f$)	(120)	102427
SBP 60	37	(TE)	-	-	278 ($i = s$)	(60) 53	277515
SBP 120	36	(TE)	-	-	590 ($i = s$)	(120) 125	64686
PA 25–35	51	(TE)	(200–400)	(200–400)	-	(25–35)	242779
PA 80–110	46	(TE)	(350–1000)	(350–1000)	-	(80–110)	145490
slit TE 1	(17)	(TE)	(30000)	(50–150)	-	-	-
slit TE 2	(29)	(TE)	(30000)	(150–250)	-	-	-

parallel to the mid section of the wing. Close to the leading edge the taps are clustered to increase resolution of the suction peak.

The TE region of the model baseline configuration can be replaced by different porous inserts (cf. Figure 3) and is not instrumented. These exchangeable parts are 0.3 m in span and their flow-permeable aft portion occupies 10 % of the chord length (i. e. chordwise extent: 30 mm). To account for the different material groups three different kinds of such porous inserts were manufactured (cf. Figure 3):

1. hollow inserts, composed of porous cover sheet material (MPP, SFF) which is internally supported by ribs,

2. solid porous inserts where the TE was cut out of a porous block by wire cut electric discharge machining (SBP, PA), and

3. streamwise slotted inserts (slit TEs), composed of spanwise alternating 0.5-mm ribs and 0.1-mm or 0.2-mm slits, respectively.

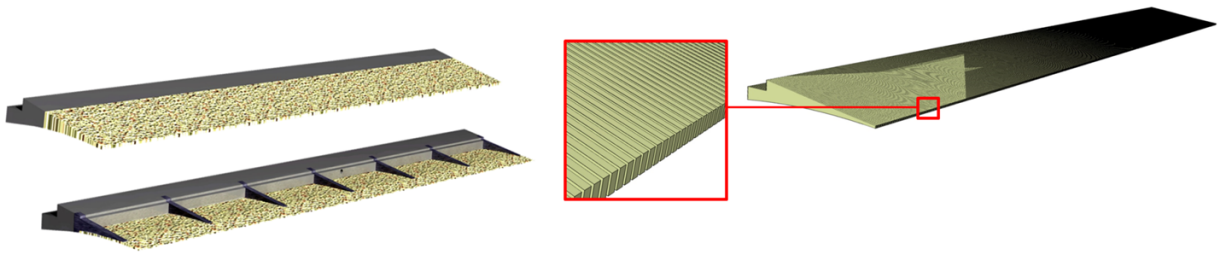

Figure 3. Realization of the porous area as solid porous part (top left) or as planked, hollow insert (bottom left with upper skin made invisible). Slotted TE insert (right).

Since the slit TEs were manually manufactured Table 1 accounts for the largest deviations from the nominal values. The non-porous reference TE thickness is $h = 1.12$ mm, whereas for manufacturing reasons (finite sheet material thickness and pore sizes), TE thicknesses h of the porous inserts show deviations from this nominal value. Approximate values are provided in Table 2 along with hypothetic local TE flow resistivities $R^0_{TE} = 2t\,R$ ($2t = h$ for MPP, but $2t \neq h$ for SFF) or $R^0_{TE} = hR$ (SBP, PA), respectively, when simply assuming the local functional layer thickness at the TE position as representative thickness value.

Table 2. TE thicknesses h, specific sheet metal resistivities R^0, and hypothetic local specific resistivities at the TE R^0_{TE}. For PA 80–110 h is ill defined due to the comparatively large pore size (maximum $w_p = l_p \approx 1$ mm).

configuration	h, mm	$R^0 = R\,t$, Ns/m^3	R^0_{TE}, Ns/m^3
reference	1.12	∞	∞
MPP 1	0.98	43	87
MPP 3	1.28	150	301
MPP 4	1.10	422	844
SFF 50	2.00	68	137
SFF 120	1.60	28	55
SBP 60	1.12	-	311
SBP 120	1.12	-	72
PA 25–35	1.12	-	272
PA 80–110	< 1.12	-	< 163

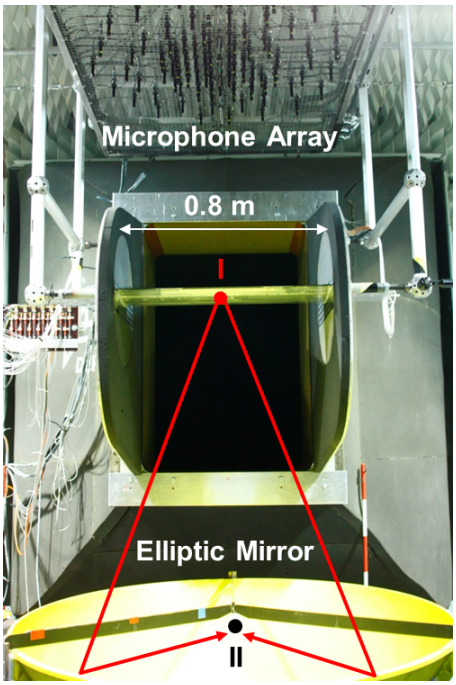

Figure 4. Test setup for acoustic measurements in the AWB.

The boundary-layers were tripped at 5 % chord length at the airfoil suction side (SS) and at 10 % chord length at the pressure side (PS), using a 0.2-mm thin zigzag tape. A stethoscope was used to verify the effectiveness of the tripping devices, ensuring a fixed transition line and, hence, reproducible TBL development along the chord.

Acoustic data were acquired through an elliptical mirror system (1.4 m reflector diameter) pointing to the PS and an additional microphone array (96 microphones) pointing to the SS to determine the noise radiated to either side for frequencies above a lower limit of 1 kHz. The current report restricts to the elliptic mirror data; farfield TE noise spectra are displayed in a 1/3-octave band format and refer to a 1-m wetted effective TE span, a 1-m observer distance, and an "overflight" TE observation direction normal to the AWB nozzle center line. For a detailed documentation of the respective acoustic mirror test setup and data correction procedures cf. Herr.[26,27]

From resolution calibrations of the mirror system it is expected that TE noise spectra for the low-noise devices will be contaminated in the lower frequency range. A major problem with regard to the current AWB model setup is that the junctions between the model and side-plate support provide strong extraneous noise sources which—due to the broadened mirror diffraction patterns at lower frequencies—can not be clearly separated from the much weaker TBL-TE noise source at the midspan measurement position. For nonzero angles-of-attack where these corner sources increase in intensity contaminations of the spectra in the current study are expected for $f_m \leq 2$ kHz. A dedicated analysis of corresponding microphone array source maps (not shown herein) revealed that these artefacts are much more critical for this specific setup than systematic errors as caused by the limited spanwise extent of the porous devices. Indeed, also clas-

sical TE noise that is generated by the untreated TE areas at the airfoil's side portions contaminates the measurement at the midspan TE position,[26,27] however, the related effects are here negligible due to the existence of the much stronger corner sources. The latter statement was confirmed by cross checks with a full-span low-noise treatment (namely for PA 80–110), exactly reproducing the measured spectra for the corresponding reduced 300-mm span insert.

In a second turn of experiments supplementing aerodynamic data were acquired in the low-speed wind-tunnel MUB of the TU Braunschweig. The MUB is a closed-return atmospheric tunnel with three different exchangeable test sections. With the applied 1.3 m by 1.3 m closed test section a maximum speed of 60 m/s is achieved. Lift polars were acquired with a repeatability of $c_l \pm 0.016$ by integration of the measured static pressure distributions. Hysteresis checks were performed by running the polar measurements for increasing and subsequently decreasing angles-of-attack α.

Moreover, detailed flow fields close to the TE were acquired by use of three-component particle image velocimetry (PIV). Data from these tests are still in the postprocessing phase and will be subject to future publications.

III. Results

III.A. Reference Configuration

Figure 5 (left) displays the measured pressure distributions for varying geometrical test angles-of-attack α_{WT} in the AWB and provides comparisons with 2D XFOIL simulations resulting in approximately identical lift coefficients. The correspondingly derived equivalent (free air) aerodynamic angles-of-attack α are used to calculate the TBL thicknesses at the TE position as listed in Table 3. These were applied to predefine the chordwise porous extent[j] in the design phase of the experiment, as well as for initial noise scaling approaches. Figure 5 (right) demonstrates the direct comparability of effective α, set in the MUB closed test section.

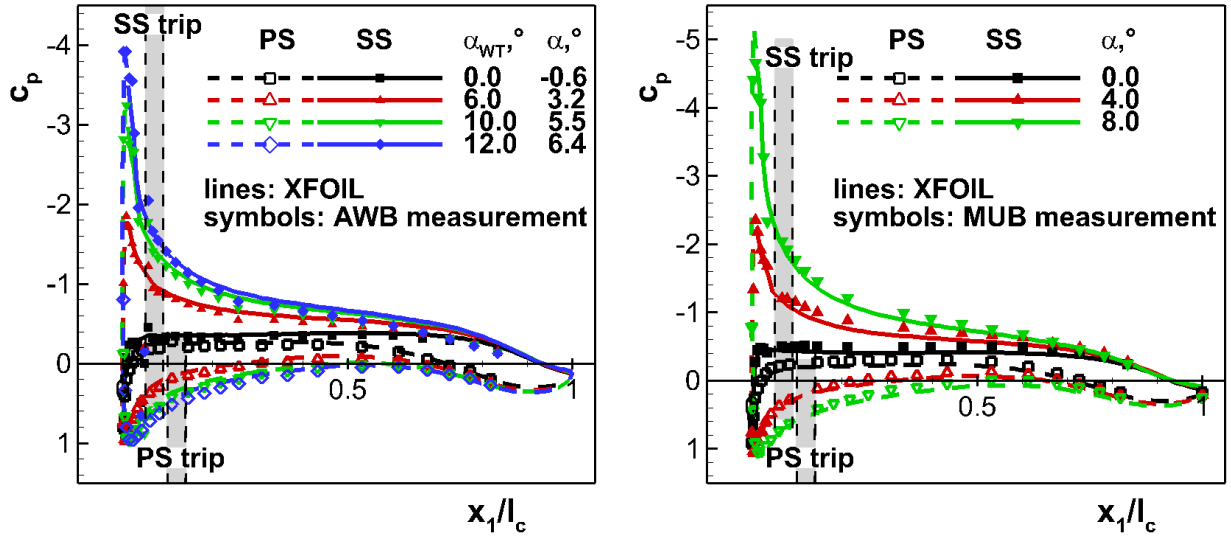

Figure 5. Comparisons of measured c_p distributions with corresponding results from XFOIL computations ($u_\infty = 50$ m/s). AWB data (left) vs. MUB data (right).

[j] Analogue to the application of alternative flow-permeable devices like e. g. brush-type TE-extensions or serrations a minimum chordwise extent of the porosity of about 1–2 δ_{SS}[27] is assumed to apply also to porous TE treatments with more anisotropic distributions of pores.

Table 3. Maximum reference TBL thickness δ_{SS} at the SS, and δ_{PS} at the PS (in brackets) in mm, XFOIL data.

		u_∞, m/s		
α_{WT}	α	40	50	60
0	-0.6	8.81 (8.00)	8.50 (7.73)	8.26 (7.52)
6	3.2	11.11 (6.54)	10.70 (6.33)	10.43 (6.17)
10	5.5	13.73 (5.79)	13.19 (5.61)	12.84 (5.47)
12	6.4	14.96 (5.52)	14.38 (5.35)	13.93 (5.22)

Figure 6 surveys the measured TE noise farfield 1/3-octave band spectra for the solid TE reference configuration. Herein, reference spectra are compared to the publicly available AWB measurement data sets that are in common use for TBL-TE noise computation benchmarks.[29,30]

Under approximately zero-lift conditions (top left subfigure) measured TBL-TE noise for the reference configurations is of comparable order as for a 0.4-m chord NACA0012-derivative airfoil. Due to the finite 1.12-mm TE thickness the respective noise spectra feature characteristic blunt TE (BTE) noise broadband humps, related to von-Kármán-type vortex-shedding from the TE. In the top right subfigure these data sets are presented in a normalized manner according to:

$$L_{p(1/3)norm} = L_{p(1/3)} - 50\log(M_\infty) - 10\log(\delta_{SS}\, b/r^2), \quad (1)$$

$$St = f_m\, \delta_0/u_\infty. \quad (2)$$

Eq. 1 applies the theoretical result of Ffowcs Williams and Hall[31] according to which farfield TE noise mean-square sound pressures $\langle p'^2 \rangle$ increase with the 5$^{\text{th}}$ power of flow Mach number M_∞. Moreover, a linear increase of $\langle p'^2 \rangle$ with a characteristic TBL length scale is assumed, here taken as δ_{SS} to scale the broadband TBL-TE noise maxima. A simple Strouhal relationship for frequency scaling is defined in Eq. 2. The characteristic scaling length δ_0 has been exceptionally set equal to the TE thickness $h = 1.12$ mm, confirming typical BTE vortex-shedding noise St of about $f_m\, h/u_\infty \approx 0.1$ in this representation format. As documented in the bottom subfigures, BTE noise humps appear to vanish for nonzero angles-of-attack.[k]

Unscaled spectra for varying α are presented at the left while scaled data (now applying also $\delta_0 = \delta_{SS}$ in the St relationship) are presented on the right. As already reported earlier[26,27] spectral peaks are shifted towards lower frequencies for increasing α, corresponding to an increase in δ_{SS}. Note that the applied scaling approach fairly brings TBL-TE noise peak regions to collapse. DU-96-180 benchmark data acquired under similar test conditions are also displayed here for informal reasons.

III.B. Effect of Porous Inserts

In consistency with previous AWB measurements at flow-permeable TE modifications[19,26,27] the same $\langle p'^2 \rangle \propto {u_\infty}^5$ velocity scaling dependence was observed for the porous inserts in the current study. Therefore, the following discussion will concentrate on results for one test velocity ($u_\infty = 50$ m/s) only. An overview of the achievable TBL-TE noise reduction potential at $\alpha = -0.6°$ is shown in Figure 8 with the data categorized according to different material groups.

For specific parameter variants, representatives from each of the selected material groups (MPP, SFF, SBP and PA) can achieve a significant broadband noise reduction potential of maximum order 6 dB which approximately corresponds to the assumed low-noise reference, herein represented by the slit TE configurations (centered right subfigure).

Along with the material characteristics listed in Tables 1 and 2 acoustic results indicate that mainly the TE flow resistivity R^0_{TE} and the spanwise pore/slit dimension w_p (or, alternatively, the effective pore diameter d_p, if w_p-values are not accessible) are the most suitable material parameters to reflect the observed global trends for all tested TE variants. A direct effect of the material porosity ϕ (separable from indirect

[k] According to a dedicated study by Herr[27] spectra are still affected by the TE bluntness at nonzero angle-of-attacks, although humps are not obviously visible. Particularly, spectra for sharp TE airfoils are expected to provide higher broadband noise levels beyond the BTE shedding-frequency.

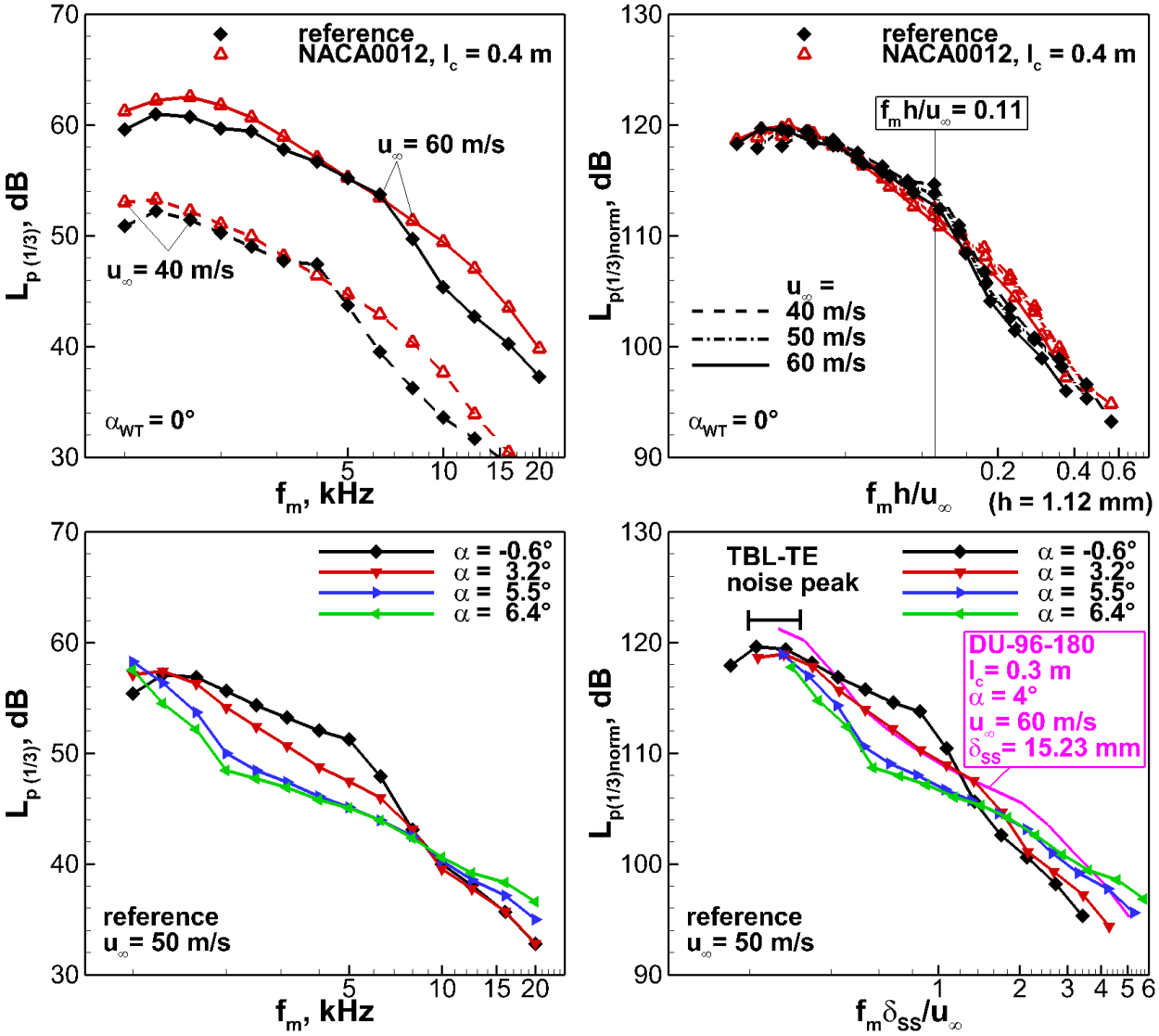

Figure 6. TE noise reference farfield 1/3-octave band spectra. Top left: Reference data compared to available benchmark data sets (NACA0012-derivative airfoil), $\alpha_{WT} = 0°$. Top right: Data sets scaled according to Eqs. 1 and 2, applying $\delta_0 = h$. Bottom left: α-dependence of reference farfield TE noise spectra. Bottom right: Comparisons of scaled reference spectra with DU-96-180 benchmark case.

effects on R_{TE}^0) can not be observed in the gained test data. Moreover, structural elements or an unfavorable distribution pattern of the porosity induce the risk of strong self noise contributions. The detailed parametric dependences deduced from Figure 8 will be described in the following.

Effect of TE Flow Resistivity on TE Noise Reduction

R_{TE}^0 determines the reduction potential over large portions of the spectra covering low-to mid frequencies up to about 10 kHz. Overall, small values of $R_{TE}^0 < 163$ Ns/m^3 led to the largest noise reduction effects, whereas for larger values the noise reduction diminishes. As a rule of thumb $R_{TE}^0 \approx 100$ Ns/m^3 are recommended for TE applications with TE thicknesses of about 1 mm at similar conditions as in the current experiment. To give an example (top left subfigure): MPP 4 with small circular holes almost restores the TE noise spectrum of the non-permeable reference configuration, whereas MPP 3 with an increased permeability provides a broadband TE noise reduction (top left subfigure). Among the MPP variants configuration MPP 1 with the largest permeability is most efficient in the lower frequency range.

Effect of Unfavorable Pore Distribution on Excess Noise Generation

When the long holes of configuration MPP 1 are streamwise aligned, strong quasi-tonal excess noise contributions are produced at higher frequencies. The latter disappear for a spanwise hole alignment (top right subfigure). This result is at first view surprising, expecting a generally improved acoustic performance for anisotropic materials with a streamwise alignment of pores. A detailed tape study (while masking selected portions of the porous insert) clearly localized these excess noise sources at the PS of the insert. Very likely, these unwanted contributions are attributable to an unfavorable hole pattern shown in Figure 7.

It is suspected that regular vortex-shedding noise is particularly produced by flow across the distinct bars between neighboring hole rows. Accordingly, these various subsumed quasi-tones do not appear when the pores are oriented perpendicular to the flow, i. e. when the bars are aligned with the mean flow direction. Material self noise contributions of such type might be generally easily avoided by e. g. a staggered distribution of holes or a significantly increased length l_p of the long holes compared to the bars. Alternatively, the thickness of the bars might be reduced to shift the quasi-tonal contributions towards higher frequencies.

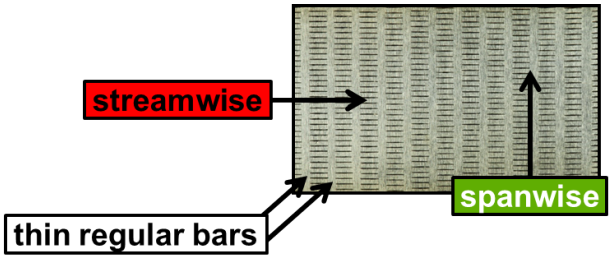

Figure 7. Photographic view of MPP 1 hole pattern with thin bars between adjacent hole rows.

Effect of Spanwise Pore Dimensions on Excess Noise Generation

For the remaining sample materials, i. e. the SFF, SBP, PA, and slit TE variants, excess noise contributions are detectable at higher frequencies around 10 kHz and are much less expressed than for MPP 1. These contributions can be avoided when spanwise pore/slit dimensions are reduced towards values of $w_p \leq 160$ μm. Increasing w_p simply results in a larger effective wetted span to produce high-frequency excess noise. Note in the context of SFF that also cross-flow through the structural grid below the functional layer might produce extra noise; SFF 120 provides a smaller functional layer thickness t, enhancing such additional contributions.

Overall, the (low-noise reference) slit TE variants still provide the lower bound at low frequencies, as surveyed in Figure 9, where direct comparisons of the most efficient configurations are also shown for nonzero angles-of-attack. However, at mid frequencies around 4 kHz the variant PA 80-110 provides a further increased noise reduction benefit. The reason for this slightly increased efficiency (and modified spectral shape) when compared to the slit TEs is seen in a reduced effective TE thickness caused by the relatively large pore size. Instead of the nominal TE thickness of 1.12 mm a rather ill-defined, much thinner TE geometry was produced, installing a favorable (but arbitrary) gradient porosity at the TE. Note that fabrication of the SBP variants proved much higher reliability in terms of required TE shape and surface quality; therefore, these variants with clear trends in measured TE noise spectra are the most recommended test cases for future use in CFD/CAA validation activities.

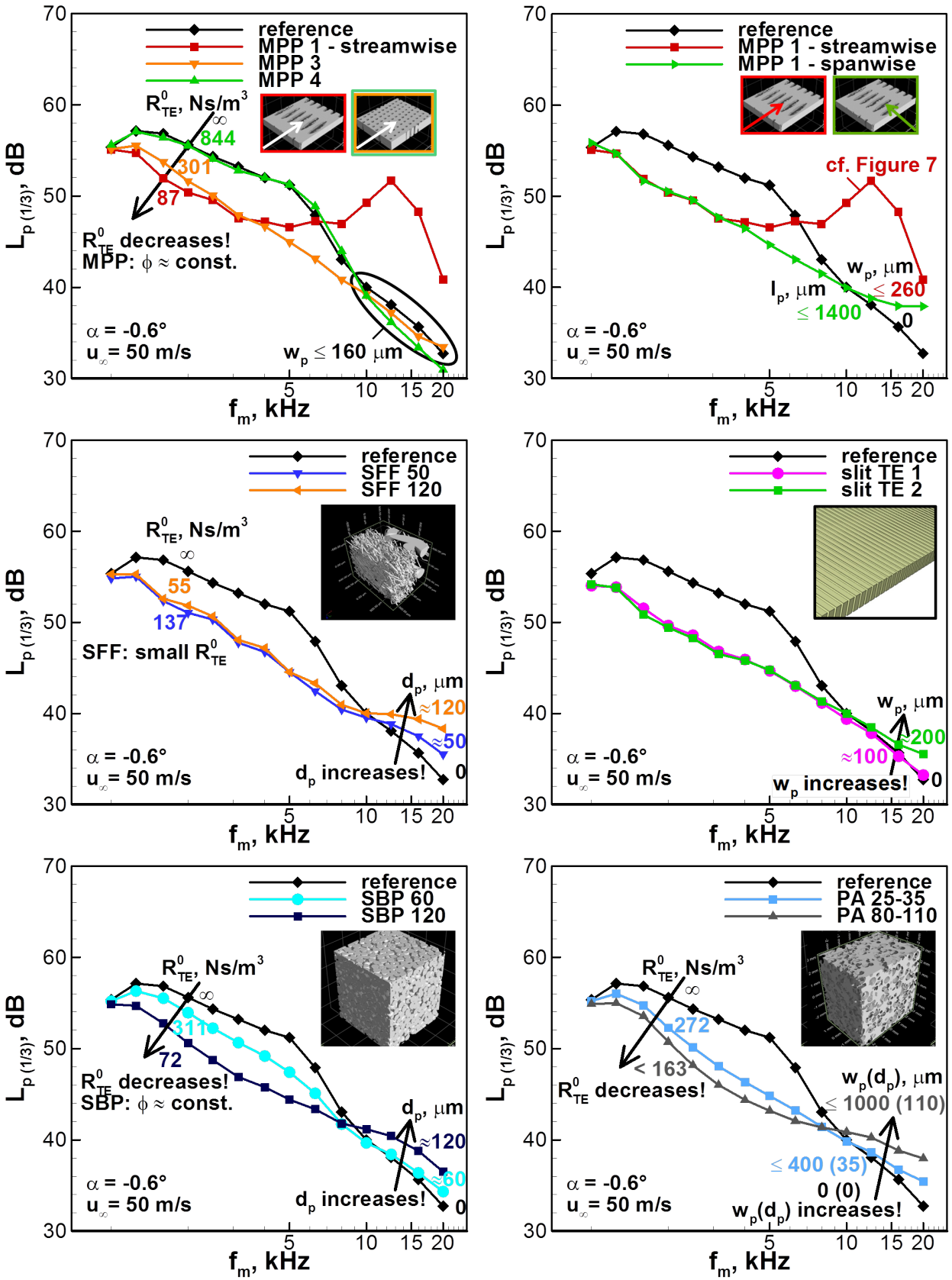

Figure 8. Effect of porous inserts on trailing-edge noise farfield 1/3-octave band spectra.

One important, still unsolved aspect is that measured TBL-TE noise reductions tend to diminish for increased airfoil loading (cf. Figure 9). This adverse α-dependence has been reported earlier,[19,20] but has not yet been finally clarified based on a pure acoustic data assessment. According to Section II.B the interpretation of the observed effects is ambiguous due to the extraneous (corner source) noise contamination of the spectra at lower frequencies where the TBL-TE noise maxima and hence, maximum noise reduction effects are expected. In this context the interested reader might refer to Herr[27] showing scaled TBL-TE noise spectra for a slit TE configuration (equivalent to slit TE 1 of the current study) applied at a NACA0012-derivative airfoil. For this case with apparently more favorable signal-to-noise ratios a broadband TE noise reduction was documented over a much larger frequency range also for nonzero angles-of-attack. Noise reductions were also larger at the higher frequencies because the reference airfoil provided a sharp TE with much higher TE noise levels at frequencies beyond the BTE shedding frequency in the current experiments.

In addition to these setup-related uncertainties it is suspected that the increased surface roughness will lead to higher kinetic energy of turbulence in the TE region, partly counterbalancing the achieved noise reduction effect. Moreover, both the surface roughness and the net cross-flow through the porous devices might provoke a case-dependent thickening/displacement of the SS TBL and an accordingly shifted noise maximum towards lower frequencies, where data reliability is limited. In this regard the recently acquired PIV data will help to clarify the local flow characteristics and hence, to gain a deeper insight into the underlying source mechanisms and noise scaling dependences.

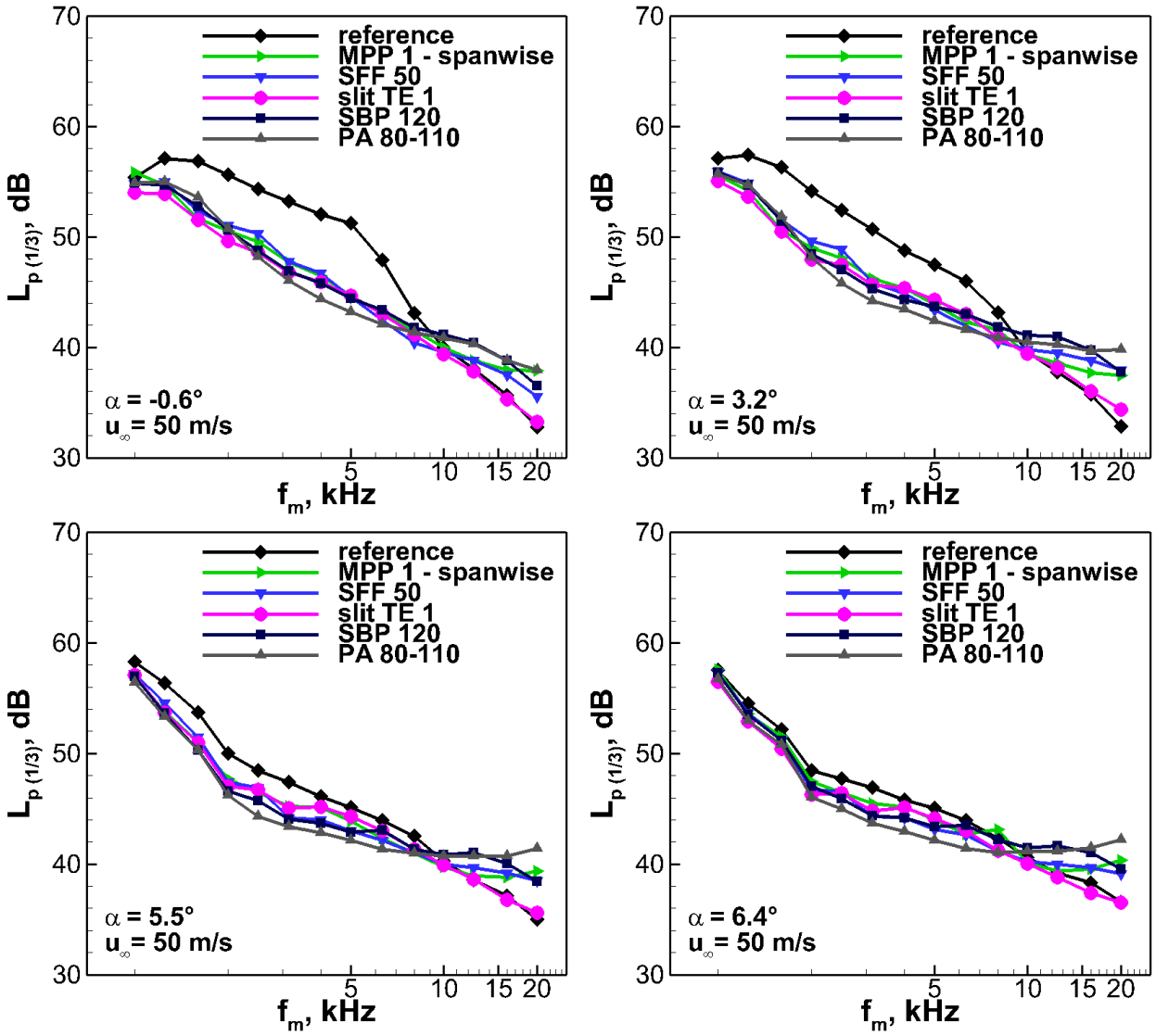

Figure 9. Effect of angle-of-attack on the achieved noise reduction benefit of selected TE materials.

Figure 10 (left) surveys TE noise spectra for SBB 120 at varying angles-of-attack; the reader might refer to Figure 6 (bottom left) for a direct comparison with the corresponding reference data. Initial results from a simple tape study at $\alpha = 3.2°$ are shown in Figure 10 (right), indicating that neither a mere surface impedance adjustment (i. e. allowing velocity fluctuations to be nonzero at the surface approaching the TE) nor acoustic absorption are sufficient to achieve a TE noise reduction effect. Sealing of either the SS or PS of the porous treatments by means of masking tape leads to the full elimination of the gained noise reduction benefit, supporting the conjecture that a pressure release *across the TE region* has to be installed. This statement has been already anticipated by dedicated theoretical and numerical studies with targeted selection of parameters under review (like e. g. neglecting viscosity in the simulation) performed by Delfs, Faßmann and Ewert[1]. Note again, that according to Figure 10 (right) the source region of high-frequency self noise generation can be clearly localized at the PS.

Since the through-flow appears to be the major requirement to achieve a noise reduction a decrease of the aerodynamic performance is expected for any kind of porous material application, when simply replacing and not extending the original TE region. Hence, integration efforts should aim at minimizing these aerodynamic deficits, or—if the installation situation allows—porous extensions of the original TE geometry might be used instead.

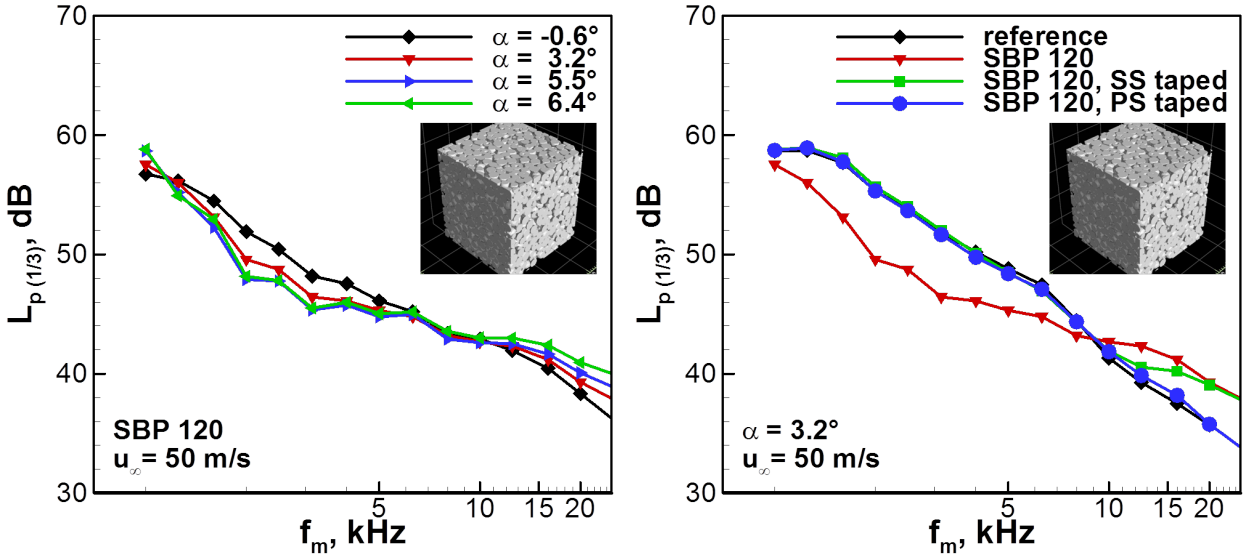

Figure 10. Noise reduction effect through variant SBP 120 (sintered bronze powder). Left: Angle-of-attack dependence of farfield TE noise spectra. Right: Effect of preventing pressure release across the porous insert by taping either the SS or PS of the porous insert.

The respective effects on the lift polars, as measured in the MUB closed test-section wind-tunnel, are shown in Figure 11. Obviously, all of the tested porous inserts induce the anticipated drop-off in lift performance. Effects are smallest for the porous block materials with larger R^0_{TE}. Nonetheless, the acoustic results are not perfectly reflected in the form of a reverse rank order such that acoustically most efficient materials with small $R^0_{TE} \approx 100$ Ns/m^3 perform aerodynamically worst or vice versa. At first view one could conclude that increasing local flow resistivity upstream of the TE related to increasing material thickness might be the cause for these inconsistencies. However, the fact that configuration MPP 4 with an almost impermeable surface (and no measured noise reduction) shows a lift performance comparable to MPP 1 indicates that lift polars for the planked TE modifications (MPP, SFF) are to a large extent influenced by small geometric deviations when compared to the reference configurations. In this context the reader might also refer to the relatively large deviations in h surveyed in Table 2 for the SFF variants.

[1]Private communication, results not yet published.

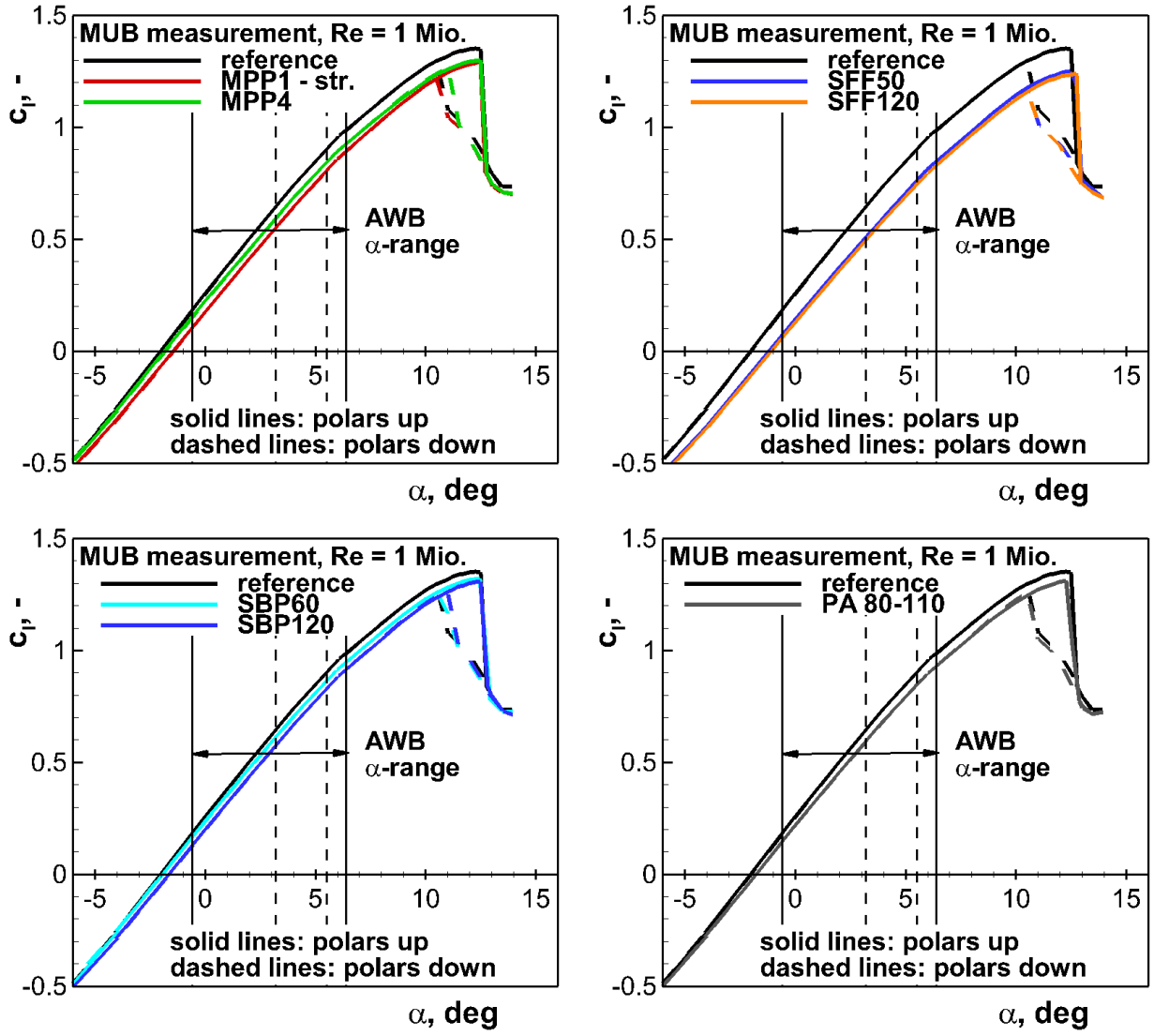

Figure 11. Lift polars for selected configurations (data not available for all TE materials).

IV. Conclusions and Outlook

The current study examines the effect of porous material application with the purpose of turbulent boundary-layer trailing-edge (TBL-TE) noise reduction. To identify the parametric dependence between material characteristics, noise reduction efficiency and aerodynamic performance the herein conducted experiments comprised

- a detailed microstructural characterization of the applied materials by means of 3D computer tomography and 2D light microscopy image analysis,
- measurements of the flow resistivity,
- noise measurements at a test airfoil (DLR F16 profile at $Re = 0.8 \times 10^6$ to 1.2×10^6) in the open-jet Acoustic Wind Tunnel Braunschweig (AWB) of DLR,
- corresponding lift and drag polar measurements in the MUB (Modell-Unterschallkanal Braunschweig) low-speed facility with closed test section at the TU Braunschweig.

The main focus in the current report is set on the documentation of the acoustic test results. As has been reported earlier in the framework of forerunner studies and confirmed once again herein, porous or slotted TE treatments used as a replacement of the rear portion of an airfoil can achieve a maximum broadband noise reduction of order 2–6 dB. TE noise spectra for porous TEs were also confirmed to follow the typical $(\text{velocity})^5$ increase of sound intensity as generally observed in the solid reference case. Apart from these more general statements major findings on the governing test parameters and functional mechanisms are summarized as follows:

- The noise reduction by means of porous TE treatments is considered mainly attributable to a material-dependent pressure release process in the acoustic nearfield, as deduced from the observation that taping of either the suction or the pressure side of the porous treated TE region fully eliminates the noise reduction benefit. Therefore, a decrease of the lift performance can not fully be avoided provided portions of the originally solid TE are replaced and not extended by the porous material.
- This material-dependence is—to a large extent—characterized by the flow resistivity of the TE material. A tentative approach, assuming the local functional layer thickness at the TE as a suitable reference length has led to the definition of a *hypothetic specific flow resistivity for TE applications*, R^0_{TE}. For porous block material this reference thickness corresponds to the TE thickness or alternatively, when porous sheet metal is applied as a porous skin, to twice the material's functional layer thickness.
- R^0_{TE} determines the noise reduction potential (observable at low- to mid frequencies up to about 10 kHz in the current study), whereas direct effects of the material porosity for given values of R^0_{TE} are not observed. Throughout the whole study—i. e. applying a large range of different porous metals with varying pore morphologies, sizes and distribution patterns—small values of $R^0_{TE} \approx 100$ Ns/m^3 led to the acoustically most beneficial results (for TE thicknesses of about 1 mm).
- High-frequency excess noise contributions are observed only for materials with comparatively large spanwise pore dimensions or with an unfavorable distribution pattern of pores. Excess noise is predominantly generated at the pressure side of the porous devices. For streamwise slots, extending over the whole TE region, or distributions of pores with spanwise dimensions $w_p \leq 160$ μm no excess noise is generated at frequencies of interest ≤ 20 kHz. Pore/slit widths of $w_p \approx 100$ μm are recommended as a suitable target value to avoid these extra noise contributions. Large regular solid structural parts (e. g. perforated plates with repetitive large support ribs separating perforated areas) have to be strictly avoided.

Still open questions remain concerning the observed adverse angle-of-attack (α) behavior; the TE noise reduction is dramatically diminished when increasing α. This observation might be erroneous and rather the consequence of limitations of the applied experimental setup. It is suspected that existent noise reduction effects at low- to mid frequencies might be masked by increasing excess noise contributions originating at the model/side-plate junctions (corner vortices increase with α). The exact assessment of the α-dependent trustworthy frequency ranges and potentials to improve the current setup will be subject to further work

along with the detailed analysis of aerodynamic effects (e. g. TBL displacement) induced by the through-flow of the devices. Supplementing particle-image-velocimetry (PIV) data as have been recently acquired in the MUB facility are still in the post-processing phase and will be reported elsewhere. These detailed flow-field measurements will provide mean velocity profiles, integral boundary-layer parameters, distributions of turbulence kinetic energy and Reynolds stresses within the TBL close to the TE.

Overall, the completed data set will be used for the validation of both aerodynamic and acoustic codes, that are currently further-developed to account for the behavior of porous materials in numerical predictions. Supporting systematic numerical studies to finally verify and rank order the potential noise reduction mechanisms at work have been already initiated within the SFB 880 activities. It is believed that CAA methodology can be effectively used within future porous TE design optimization efforts and will considerably help to enhance the common state of knowledge. Future research activity will include the evaluation of the effects of material and flow anisotropy on TBL-TE noise. The design and testing of tailored materials with gradual porosity is solicited.

Acknowledgments

The present work was conducted within the framework of the Collaborative Research Center *SFB 880—Fundamentals of High-Lift for Future Civil Aircraft* funded by the *Deutsche Forschungsgemeinschaft* (DFG).

References

[1]Radespiel, R. and Heinze, W., "SFB880– Fundamentals of High-Lift for Future Commercial Aircraft," *Deutscher Luft- und Raumfahrtkongress*, Stuttgart, 2013.

[2]Hayden, R. E. and Chanaud, R. C., "Foil Structures with Reduced Sound," United States Patent 3,853,428, Dec. 10, 1974.

[3]Fink, M. R. and Bailey, D. A., "Airframe Noise Reduction Studies and Clean-Airframe Noise Investigation," NASA Contractor Report CR-159311, April 1980.

[4]Fink, M. R. and Bailey, D. A., "Model Tests of Airframe Noise Reduction Concepts," AIAA Paper 80-0979, June 1980.

[5]Khorrami, M. R. and Choudhari, M. M., "Application of Passive Porous Treatment to Slat Trailing Edge Noise," NASA TM- 2003-212416, May 2003.

[6]Ma, Z., Smith, M., Richards, S. K., and Zhang, X., "Slat Noise Attenuation Using Acoustic Liner," AIAA Paper 2005-3009, May 2005.

[7]Ma, Z. and Zhang, X., "Numerical Investigation of Broadband Slat Noise Attenuation with Acoustic Liner Treatment," *AIAA Journal*, Vol. 47, No. 12, Dec. 2009, pp. 2812–2820.

[8]Angland, D., Zhang, X., Chow, L. C., and Molin, N., "Measurements of Flow around a Flap Side-Edge with Porous Edge Treatment," AIAA Paper 2006-213, Jan. 2006.

[9]Dobrzynski, W., Gehlhar, B., and Buchholz, H., "Windkanalstudien zur Eigengeräuschminderung an Verkehrsflugzeugen," Internal DLR Report IB 129-2000/11, 2000.

[10]Drobietz, R. and Borchers, I., "Generic Wind Tunnel Study on Side Edge Noise," AIAA Paper 2006-2509, May 2006.

[11]Revell, J. D., Kuntz, H. L., Balena, F. J., Horne, C., Storms, B. L., and Dougherty, R. P., "Trailing-Edge Flap Noise Reduction by Porous Acoustic Treatment," AIAA Paper 97-1646-CP, March 1997.

[12]Bohn, A. J., "Edge Noise Attenuation by Porous-Edge Extensions," AIAA Paper 76-0080, Jan. 1976.

[13]Hayden, R. E., Scharton, T. D., Kadman, Y., Wilby, J., and Rudd, M. J., "A Preliminary Evaluation of Noise Reduction Potential for the Upper Surface Blown Flap," NASA Contractor Report CR-112246, 1972.

[14]Lowson, M. V., "Reduction of Compressor Noise Radiation," *Journal of the Acoustical Society of America*, Vol. 43, No. 1, 1968, pp. 37–50, DOI: 10.1121/1.1910760.

[15]Potter, R. C., "An Experiment to Examine the Effect of Porous Trailing Edges on the Sound Generated by Blades in an Airflow," NASA Contractor Report 66565, Wyle Laboratories, Report WR 68-6, March 1968.

[16]Khorrami, M. R., Lei, F., and Choudhari, M. M., "Novel Approach for Reducing Rotor Tip-Clearance-Induced Noise in Turbofan Engines," *AIAA Journal*, Vol. 40, No. 8, August 2002, pp. 1518–1528.

[17]Geyer, T., Sarradj, E., and Fritzsche, C., "Zur Minderung des Umströmungsgeräusches bei Profilen aus porösem Material," *Fortschritte der Akustik - DAGA 08*, Vol. 2008, 10–13 March 2008, pp. 297–298, CD Conference Paper, 34. Jahrestagung für Akustik.

[18]Geyer, T., Sarradj, E., and Fritzsche, C., "Porous Airfoils: Noise Reduction and Boundary Layer Effects," AIAA Paper 2009-3392, May 2009.

[19]Herr, M. and Reichenberger, J., "In Search of Airworthy Trailing-Edge Noise Reduction Means," AIAA-Paper 2011-2780, June 2011.

[20]Sarradj, E. and Geyer, T., "Noise Generation by Porous Airfoils," AIAA Paper 2007-3719, May 2007.

[21]Ingard, K. U. and Dear, T. A., "Measurement of Acoustic Flow Resistance," *Journal of Sound and Vibration*, Vol. 103, No. 4, 1985, pp. 567–572.

[22]Howe, M. S., "A Review of the Theory of Trailing Edge Noise," *Journal of Sound and Vibration*, Vol. 61, No. 3, 1978, pp. 437–465.

[23]Leppington, F. G., "The Effective Compliance of Perforated Screens," *Mathematica*, Vol. 24, Dec. 1977, pp. 199–215, DOI: 10.1112/S0025579300009116.

[24]Crighton, D. G. and Leppington, F. G., "Scattering of Aerodynamic Noise by a Semi-Infinite Compliant Plate," *Journal of Fluid Mechanics*, Vol. 43, No. 4, 1970, pp. 721–736.

[25]Jaworski, J. W. and Peake, N., "Aerodynamic Noise from a Poroelastic Trailing Edge with Implications for the Silent Flight of Owls," AIAA Paper 2012-2138, June 2012.

[26]Herr, M., "Design Criteria for Low-Noise Trailing-Edges," 13th AIAA/CEAS Aeroacoustics Conference, Rome, Italy AIAA-Paper 2007-3470, 21–23 May 2007.

[27]Herr, M., *Trailing-Edge Noise—Reduction Concepts and Scaling Laws*, Doctoral thesis, Fakultät für Maschinenbau, Technische Universität Braunschweig, Germany (published as DLR Report 2013-32, ISRN DLR-FB–2013-32), 2013.

[28]Pott-Pollenske, M. and Delfs, J., "Enhanced Capabilities of the Aeroacoustic Wind Tunnel Braunschweig," AIAA Paper 2008-2910, May 2008.

[29]Herr, M., Bahr, C., and Kamruzzaman, M., "Workshop Category 1: Trailing-Edge Noise," Problem Statement for the AIAA/CEAS Second Workshop on Benchmark Problems for Airframe Noise Computations (BANC-II), June 7–8 2012, Colorado Springs, Colorado, USA, URL: https://info.aiaa.org/tac/ASG/FDTC/DG/BECAN_files_/BANCII_category1, June 2012.

[30]Herr, M. and Kamruzzaman, M., "Benchmarking of Trailing-Edge Noise Computations—Outcome of the BANC-II Workshop," AIAA-Paper 2013-2123, May 2013.

[31]Ffowcs Williams, J. E. and Hall, L. H., "Aerodynamic Sound Generation by Turbulent Flow in the Vicinity of a Scattering Half Plane," *Journal of Fluid Mechanics*, Vol. 40, No. 4, 1970, pp. 657–670.